ISSN 1061-933X, Colloid Journal, 2018, Vol. 80, No. 6, pp. 792–802. © Pleiades Publishing, Ltd., 2018.
Original Russian Text © Yu. Yamauchi, I.V. Blonskaya, P.Yu. Apel, 2019, published in Kolloidnyi Zhurnal, 2019, Vol. 81, No. 1, pp. 125–136.

Osmosis in Negatively Charged Nanocapillaries and Its Enhancement by an Anionic Surfactant

Yu. Yamauchi[a], I. V. Blonskaya[a], and P. Yu. Apel[a, b, *]

[a]*Joint Institute for Nuclear Research, Dubna, Moscow oblast, 141980 Russia*
[b]*Dubna State University, Dubna, Moscow oblast, 141982 Russia*
**e-mail: apel@jinr.ru*

Received July 16, 2018

Abstract—Osmotic flows through track-etched membranes with pore radii of 10–50 nm have been measured in a water/membrane/salt solution system at a salt concentration on the order of several millimoles per liter. It has been found that water is intensely transported through the pores only when a solute dissociates into ions (KCl, K2SO4, sodium dodecyl sulfate, etc.). Molecules of low-molecular-mass nonelectrolytes induce actually no osmotic flows at these capillary radii, thereby indicating the key role of an electrical double layer in the mechanism of the osmotic transport. It has been shown that the transport through the pores under the action of the osmotic pressure is of a convective nature; i.e., the Poiseuille law for a viscous flow through a cylindrical capillary is fulfilled. The values of the osmotic pressure have been determined at different salt concentrations, and reflection coefficients have been calculated. The reflection coefficients correlate with the values of apparent diffusion coefficients of salts in nanopores, and these diffusion coefficients are markedly smaller than bulk values. The sorption of an anionic surfactant increases the membrane surface charge and enhances the osmotic effect.

DOI: 10.1134/S1061933X19010162

1. INTRODUCTION

Osmosis is the flow of a solvent, e.g., water, through a semipermeable membrane from a region with a low concentration of a solute to the region of its higher concentration. In the nature, this phenomenon is of great importance for transport processes occurring in plants and living organisms, and, in modern technologies, it is used for, e.g., separation of mixtures or the generation of "green" electric energy [1, 2]. In spite of the fact that osmosis has been known for a long time and studied since the 19th century [3–10], its nature remains to be completely understood. Several models are employed for explaining osmosis mechanism, including erroneous ones, which, nevertheless, pass from one communication to another. The historical review of this phenomenon and the analysis of the contemporary notions are presented in, e.g., [11–13]. It is traditionally believed that osmosis is characteristic of semipermeable membranes, i.e., membranes which almost completely reject molecules of a solute. Therefore, in the case of porous ("capillary") membranes, experiments on osmosis have been carried out only with solutions of high-molecular-mass compounds [7, 14, 15]. This situation has resulted from the entrenched opinion that "the osmotic pressures of lipid-insoluble solutes are effective across cell membranes, whereas only osmotic pressures of macromolecular solutes are effective across capillary membranes" [7].

However, experiments recently performed with asymmetric track-etched membranes (**TMs**) have shown that the strongly pronounced osmotic effects may be observed for solutions of low-molecular-mass salts in pores with radii of a few nanometers to several tens of nanometers [16, 17]. It has been found that conical pores resulting from asymmetric etching [18] generate easily recorded osmotic flows at high electrolyte concentration gradients. Such pores have greatly different radii at their opposite ends (5–10 and 150–300 nm, respectively) and, therefore, exhibit a substantially lower resistance to viscous flow than cylindrical channels do [19]. This circumstance has made it possible to reveal the effect; however, it complicates in-depth study of the process, because the geometric parameters of such pores, especially of their narrow parts, have not been reliably determined.

The goal of this work was to study the basic aspects of osmosis in submicrometer channels. For this purpose, we used "conventional" TMs with cylindrical pores, which had been thoroughly characterized by several methods. Osmotic flows of water caused by solutions of both electrolytes and substances nondissociable in water were measured. In parallel, the rate of opposite solute diffusion was measured. The data obtained have made it possible to understand the main

Table 1. Basic characteristics of the track-etched membranes under investigation

Membrane	Average thickness, μm	Pore density, cm^{-2}	Q_{air}, mL cm^{-2} min^{-1}	Effective pore diameter d_{air}, nm	Q_w, mL cm^{-2} min^{-1}	Effective pore diameter d_w, nm
TM-25	10.8	8×10^9	8.7 at 10 kPa	26 ± 2	3.7×10^{-3} at 10 kPa	24 ± 1
TM-40	11.9	2.9×10^9	5.8 at 5 kPa	41 ± 2	1.0×10^{-2} at 10 kPa	41 ± 1
TM-100	9.6	1.1×10^9	120 at 10 kPa	111 ± 5	8.4×10^{-2} at 5 kPa	100 ± 3
TM-2000	17.8	2.0×10^6	3.4×10^3 at 10 kPa	$(2.1 \pm 0.1) \times 10^3$	–	–

(1) Q_{air} and Q_w are the volume flow rates of air and deionized water, respectively, at pressure drops denoted in the table. (2) The errors in the determination of the effective diameters result from the random errors in the determination of pore density, thickness and area of a membrane, and the measurement of the flow rates.

features of the osmotic process induced by the electrical double layers (**EDLs**) in the pores of TMs.

2. EXPERIMENTAL

2.1. Membranes

Poly(ethylene terephthalate) (**PET**) TMs with different pore radii were used. The membranes were obtained by irradiating PET films with heavy ions in accelerators of the Flerov Laboratory of Nuclear Reactions, Joint Institute for Nuclear Research, followed by a physicochemical treatment leading to the formation of cylindrical pores [20]. The physicochemical treatment comprised the UV irradiation (wavelength of >285 nm) followed by chemical etching in a sodium hydroxide solution. Depending on a required pore diameter, sodium hydroxide concentration and temperature were varied within ranges of 0.5–3 mol/L and 80–90°C, respectively. The membrane had the shape of a tape 320 mm wide, from which circles were cut with a diameter of 30 mm, which corresponded to the size of the sample seat in a measuring cell.

The characteristics of the membranes are presented in Table 1. The density of pores calculated per unit surface area was determined from micrographs taken with a scanning electron microscope (**SEM**). Irrespective of the number of counted pores (no less than 700), the average pore density in the samples was characterized by a confidence interval of nearly ±10%, because the conditions of the irradiation by ions did not ensure a more uniform distribution. Typical micrographs taken from the surfaces of the TMs used in the experiments are presented in Figs. 1a–1d. It should be emphasized that the size of an pore entrance does not accurately reflect the diameter of a channel, because small pores have funnel-shaped ends as a result of the action of UV radiation on the surface layer of PET. This feature may be exhibited by comparing the SEM micrographs of the surfaces and the sections of the membranes, which should be low-porosity to make the membrane internal structure distinctly evident [17].[1] Figure 1e exemplifies a membrane fragment, in which the pore channels inside of the membrane and the holes on its surface are seen simultaneously. Therefore, the effective pore diameter calculated from the data on gas or water permeability through a membrane at a low pressure drop is a more objective characteristic. Accurate measurements by this method yield very good agreement in the case of nanoporous TMs [21, 22].

Ultra- and microfiltration TMs, including in fact all of those represented on the contemporary market, are distinguished by nonparallel pore channels [22]. In our samples, the axes of the pore channels were uniformly distributed within a range of angles φ from 0° to 30° with respect to the normal. Hence, for both the diffusion transport and the viscous flow, the effective pore length was unequal to the membrane thickness. Easy calculation shows that, for the aforementioned angle range, the average cosine of the pore tilt angle is $\langle\cos\varphi\rangle = 0.956$; hence, effective length l of pore channels in the membranes is $l_0/0.956$, where l_0 is the membrane thickness. This circumstance was taken into account when calculating the effective pore diameters and the diffusion permeability of the TMs.

2.2. Measurements of Osmotic Flows and Diffusion Fluxes

The experiments were carried out in a transparent Plexiglas cell divided in the center by a partition (see Fig. 2). The left-hand part of the cell was filled with a

[1] Note that commercial polycarbonate TMs have an opposite property: the inlet diameter of the pores is commonly smaller than their internal diameter [7, 22, 23] because of specific features of their production technology.

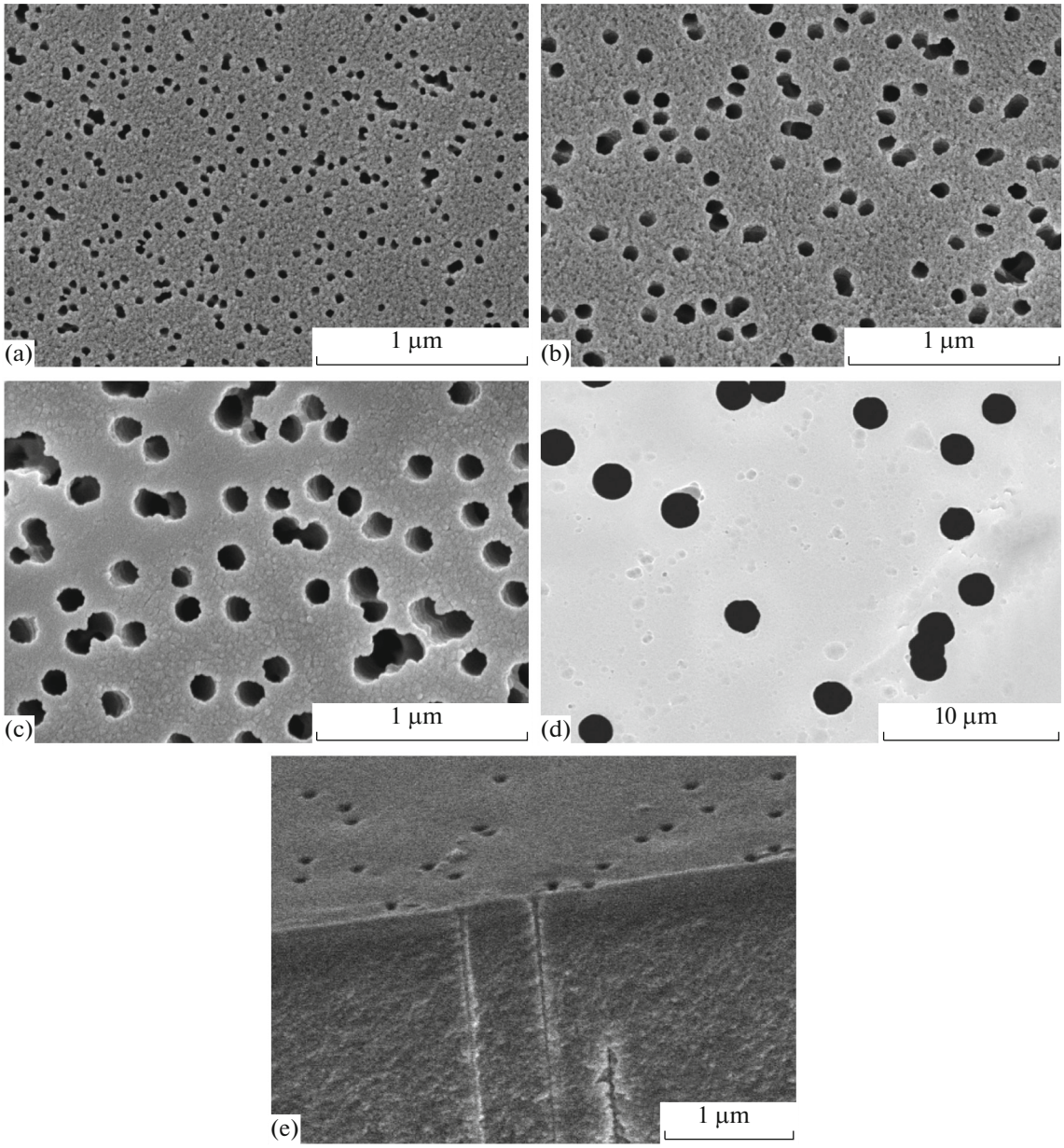

Fig. 1. Electron micrographs taken from the surfaces of different track-etched membranes: (a) TM-25, (b) TM-40, (c) TM-100, and (d) TM-2000 and (e) electron micrograph taken from a cleavage fragment of TM with an effective pore diameter of 33 nm and a pore density of 10^8 cm^{-2}.

solution having a known concentration, while the right-hand part was filled with ultrapure water prepared using an Arium system (Vladisart, Russia). A TM sample into a seat located in the partition between the parts of the cell, with the seat having a diameter of 30 mm and containing an orifice with an area of 3.14 cm^2. A new sample was taken for each experiment. The left- and right-hand parts of the cell contained a solution (300 mL) and water (250 mL), respectively. The left-hand part of the cell was equipped with a polysulfone capillary having an internal diameter of 1.00 ± 0.02 mm. Its diameter was determined from the difference between the weights of the dry and water-filled capillary 1500 mm long. The solution was intensely stirred with a Teflon-coated magnetic stirrer. The content of the right-hand part of the cell was stirred with a propeller stirrer.

After the assembly of the cell, its filling, and the onset of the stirring, the initial level of the liquid in the capillary was, as a rule, nonzero, which, however, did not hinder the monitoring of the osmotic flows. The height of the solution rise in the capillary was measured as time function $h(t)$. Maximum height h_{max} yielded the value of osmotic pressure for a given solu-

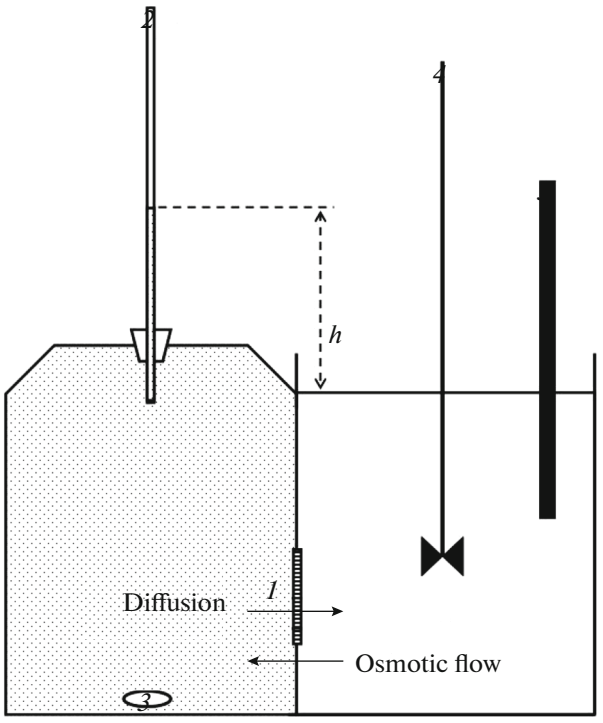

Fig. 2. Cell used for measuring osmotic flows and diffusion fluxes: (*1*) membrane, (*2*) measuring capillary, (*3*) magnetic stirrer, (*4*) propeller stirrer, and (*5*) sensor of conductometer.

tion. To measure the solution flow rate through a membrane under the action of hydrostatic pressure, water in the right-hand part of the cell was replaced by an equiconcentrated working solution, thereby equating the osmosis characteristics on both sides of the membrane. The level of the solution in the capillary began to decrease, thereby offering opportunity to measure descending function $h'(t)$. The experiments were performed at room temperature of 22 ± 1°C.

The specific conductivity in the right-hand part of the cell was monitored with a ProfLine Cond 3110 conductometer, and the concentration of the salt diffusing through the membrane was calculated. An almost linear dependence of the electrical conductivity on the salt concentration was observed under the experimental conditions (low concentrations of ≤4 mmol/L). The coefficients used to calculate the concentration from the values of the specific conductivity were 1.46×10^{-5}, 3.37×10^{-6}, and 6.83×10^{-6} (mol/L)/(μS/cm) for sodium dodecyl sulfate (**SDS**), K_2SO_4, and KCl, respectively. The error in concentration measurement was mainly governed by temperature fluctuations, which amounted to ±1°C. Diffusion of a nonionic surfactant, polyoxyethylene-4-nonylphenyl ether with 10 ethylene oxide units (**PONPE10**), was measured by periodically recording the optical absorption of the solution in the right-hand part of the cell [24]. The solutions were equilibrated with ambient air and had pH values in a range of 5.6–6.5. Membrane diffusion permeability was calculated under the assumption that stagnant layers were absent. To verify the results, several experiments on diffusion were carried out with a coarse-pore membrane (TM-2000), whose pore radius was incommensurably larger than EDL thickness. Values close to the reference volume diffusion coefficients, which are presented in the lower part of Table 4, were obtained. It should be emphasized that the procedure does not provide an error in the determination of the diffusion permeability smaller than ±10%, because variations in the membrane porosity make the decisive contribution to the total error.

3. RESULTS AND DISCUSSION

Figure 3a presents the diagrams for a rise in the solution level caused by the osmotic flow through the TM-25 membrane. Over nearly 7 h, the level reaches its maximum value h_{max}, which corresponds to osmotic pressure $\Delta\Pi_{meas}$ characteristic of an examined solution and a membrane. Figure 3b shows the time dependence of electrolyte concentration in the right-hand part of the cell, with this dependence linearly increasing throughout the period under consideration. A change in the solution volume in the left-hand part of the cell is no larger than 1 mL, while the growth of the electrolyte concentration in the right-hand part of the cell by the moment, at which h_{max} is reached, is nearly 1% of the concentration in the left-hand part of the cell. Thus, both processes—osmotic flow of water and opposite electrolyte diffusion—occur at an almost constant driving force. Such diagrams were recorded for different electrolytes taken in several concentrations and three TMs with different pore diameters. The measured values of osmotic pressure are summarized in Tables 2–4. Reflection coefficients [1–7] were calculated as the ratios between measured osmotic pressure $\Delta\Pi_{meas}$ and ideal pressure $\Delta\Pi = icRT$:

$$\sigma = \frac{\Delta\Pi_{meas}}{icRT}, \quad (1)$$

where i is a coefficient that takes into account salt dissociation, c is the molar concentration, R is the gas constant, and T is the absolute temperature.

Simultaneously with the osmotic water flow from the right-hand part of the cell to the left-hand one, an opposite diffusion transport of an electrolyte takes place. The difference between the slopes of straight lines *1* and *2* in Fig 3b substantially exceeds a factor of 2 because of different values of diffusion permeability. The tendency to a decrease in the apparent diffusion coefficient with a reduction in the concentration is observed for all three TMs with pore sizes of ≤100 nm and for all studied electrolytes (see the last columns in Tables 2–4). This regularity is due to the well known

effect of exclusion of coions from pores under the action of electric field [25]. The rupture of ester bonds in a PET film during the chemical etching of tracks leads to the formation of terminal carboxyl groups [26]. At pH > 4, carboxyl groups are dissociated; therefore, the front surface of a TM and the walls of a pore are coated with a "network" of negative elementary charges. According to the data obtained by different methods, the surface charge density in PET TMs is in a range of 0.1–1 elementary charge per 1 nm^2 [27–33].

It is obvious that EDL induces the observed osmotic effect. As follows from the experimental data, at low electrolyte concentrations, the TM with the smallest pores generates an osmotic pressure close to the ideal one (see Table 2). For example, in the case of a 1 mmol/L K_2SO_4 solution and the TM-25 membrane, the reflection coefficient is 0.87. Here, the values of the pore radius and Debye length are close to each other. As the electrolyte concentration increases, the reflection coefficient decreases due to the compression of the EDL in the membrane pores. The decisive role of the electrostatic mechanism in the osmotic effect is also evident from the finding that, at the same molar concentration of a 1 : 1 electrolyte (KCl) and a 1 : 2 electrolyte (K_2SO_4), the reflection coefficient is higher in the latter case. At the same concentrations, solutions of nonelectrolytes—saccharose and PONPE10—insubstantially change the liquid level in the measuring capillary.

It is also of interest to compare the osmotic effects caused by sorbable and nonsorbable (low-sorbable) electrolytes. Figure 4a presents the concentration dependences of the osmotic pressures measured for KCl and SDS solutions. At low concentrations (≤1 mmol/L), the osmotic pressure is the same for both electrolytes and close to the ideal osmotic pressure. When the concentration is increased to 4 mmol/L, a substantial difference arises, and the osmotic pressure of the SDS solution becomes higher. Most probably, the sorption of dodecyl sulfate anions on the TM surface increases the electric charge density. It is known that, at concentrations of about 1 mmol/L and above, dodecyl sulfate ions can be sorbed due to hydrophobic interactions [34, 35], although they are coions with respect to the negatively charged polymer surface. The sorption markedly increases when approaching the critical micelle concentration, which is equal to 8 mmol/L [35]. A rise in the surface charge density leads to an increase in the membrane selectivity according to the theoretical predictions [10]. A similar effect may be observed for 1 : 2 electrolytes and larger pores (Fig. 4b). Solutions of another surfactant, sodium dodecyl diphenyloxide disulfonate (**SDDD**), generate osmotic pressure double that of potassium sulfate solutions, with the maximum value being reached already at concentrations of 1–2 mmol/L. Note that, at c = 1 mmol/L, the Debye

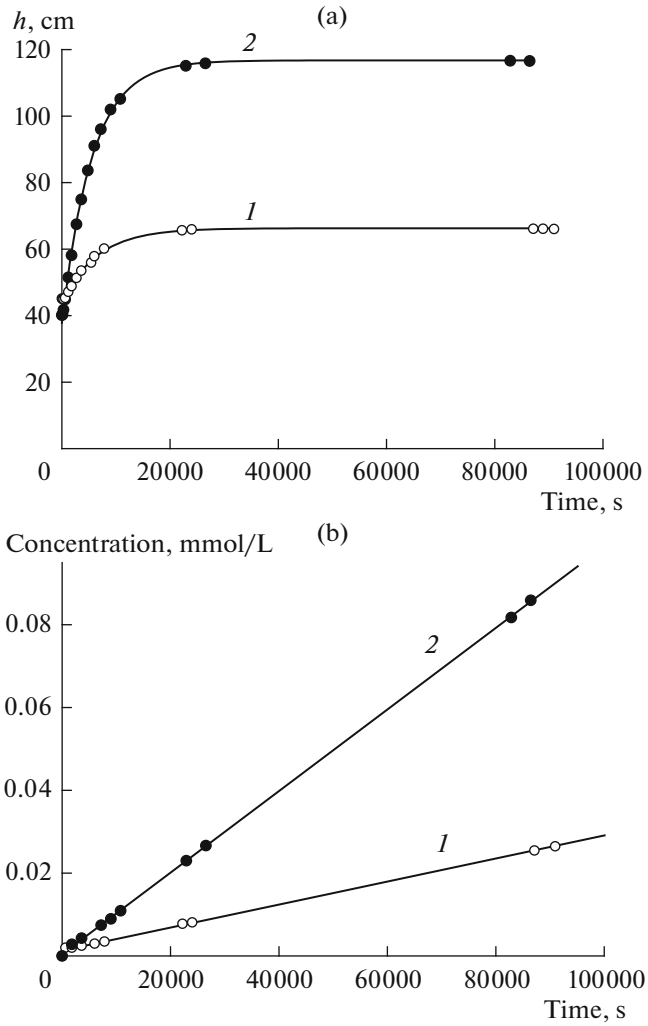

Fig. 3. Panel (a): time dependences of solution level in the left-hand part of the measuring cell for K_2SO_4 solutions with concentrations of (*1*) 1 and (*2*) 2 mmol/L and panel (b): dependences measured in parallel for K_2SO_4 concentration in the right-hand part of the cell. TM-25 membrane is under examination.

length for a 1 : 2 electrolyte is 5.6 nm, which is only ~11% of the pore radius in the TM-100 membrane. Nevertheless, the effect of anion exclusion from the pores leads to the generation of a noticeable osmotic flow. This result could be expected on the basis of the regularities for SDDD sorption in TM pores [36]. As has been established in [36], under the conditions of surfactant concentrations equal to ~0.1 mmol/L and the absence of a background electrolyte, the sorption of this surfactant in pores with an effective radius of ≈130 nm is negligible.

Let us consider the dynamics of solution column rise in the measuring capillary upon osmosis. According to the theoretical notions [1–4], volume flow rate J_v of a liquid through a membrane is determined as

$$J_v = L_p[\sigma\Delta\Pi - \Delta P], \quad (2)$$

Table 2. Osmotic pressure, reflection coefficient, and diffusion permeability of the TM-25 membrane

Solute	Concentration, mmol/L	Column height h_{max}, m	Osmotic pressure $\Delta\Pi_{meas}$, kPa	Ideal osmotic pressure, kPa	Reflection coefficient, σ	Diffusion permeability, $cm^2\ s^{-1}$
SDDD	1.00	0.636	6.21	7.38	0.84	–
	2.00	1.13	11.1	14.8	0.75	–
	4.00	1.94	18.9	29.5	0.64	–
K_2SO_4	1.00	0.661	6.45	7.38	0.87	7.0E-07
	2.00	1.14	11.2	14.8	0.76	1.3E-06
	3.95	1.70	16.6	29.2	0.57	2.6E-06
SDS	1.00	0.384	3.75	4.92	0.76	1.0E-06
	2.00	0.726	7.09	9.84	0.72	1.2E-06
	4.00	1.24	12.1	19.7	0.62	1.7E-06
KCl	1.00	0.378	3.69	4.92	0.75	2.1E-06
	2.00	0.606	5.92	9.84	0.60	4.0E-06
	4.00	0.872	8.52	19.7	0.43	5.0E-06
PONPE10	3.00	≤0.03	≤0.3	7.38	–	2.40E-07

Table 3. Osmotic pressure, reflection coefficient, and diffusion permeability of the TM-40 membrane

Solute	Concentration, mmol/L	Column height h_{max}, m	Osmotic pressure $\Delta\Pi_{meas}$, kPa	Ideal osmotic pressure, kPa	Reflection coefficient σ	Diffusion permeability, $cm^2\ s^{-1}$
K_2SO_4	0.50	0.322	3.15	3.69	0.85	1.2E-06
	1.00	0.539	5.26	7.38	0.71	2.2E-06
	2.00	0.803	7.84	14.8	0.53	3.7E-06
	4.00	0.939	9.17	29.5	0.31	6.0E-06
SDS	1.00	0.341	3.33	4.92	0.68	1.8E-06
	4.00	0.889	8.68	19.7	0.44	3.0E-06
	8.20	1.27	12.4	40.3	0.31	3.7E-06
KCl	2.00	0.405	3.96	9.84	0.40	6.4E-06
	4.00	0.611	5.97	19.7	0.30	8.0E-06
Saccharose	2.00	≤0.1	≤1	4.92	–	–
PONPE10	2.77	≤0.04	≤0.4	6.81	–	–

where L_p is the hydraulic permeability of a membrane and ΔP is the hydrostatic pressure drop across the membrane, this drop increasing with the height of the liquid rise in the capillary. Here J_v and L_p are not normalized to the unit pore area. The authors of [4] have emphasized that is a thermodynamic parameter, which is not the pressure as such; therefore, the common term "osmotic pressure" may lead to a misconception. Nevertheless, this term is generally accepted, and we use it in this article with the aforementioned stipulation.

At column height h of a liquid with density ρ, the hydrostatic pressure drop across a membrane is

$$\Delta P = hg\rho, \tag{3}$$

where g is the freefall acceleration. Introducing liquid volume Q_v in the measuring capillary and capillary cross-sectional area S_c, we express the hydrostatic pressure via these values as follows:

$$\Delta P = \frac{\rho g Q_v}{S_c}. \tag{4}$$

Taking into account that $\sigma\Delta\Pi = \Delta\Pi_{meas} = h_{max}g\rho$, and $J_v = dQ_v/dt$, we easily arrive at the following equation that describes the temporal change of the solution column height in the capillary under the action of

Table 4. Osmotic pressure, reflection coefficient, and diffusion permeability of TMs with pore diameters of 100 and 2000 nm

Membrane	Solute	Concentration, mmol/L	Column height h_{max}, m	Osmotic pressure $\Delta\Pi_{meas}$, kPa	Ideal osmotic pressure, kPa	Reflection coefficient σ	Diffusion permeability, $cm^2\ s^{-1}$
TM-100	K_2SO_4	0.25	0.050	0.48	1.84	0.26	2.3E-06
		0.50	0.108	1.06	3.69	0.29	2.9E-06
		1.00	0.124	1.21	7.38	0.16	3.6E-06
		2.00	0.111	1.09	14.8	0.07	4.4E-06
		4.00	0.115	1.12	29.5	0.04	4.5E-06
	SDS	0.26	0.036	0.35	1.26	0.28	3.1E-06
		0.51	0.081	0.79	2.52	0.31	2.9E-06
		1.03	0.088	0.86	5.04	0.17	2.5E-06
		2.05	0.111	1.08	10.1	0.11	3.0E-06
		3.08	0.165	1.61	15.1	0.11	2.9E-06
		4.10	0.190	1.86	20.2	0.09	2.8E-06
		8.20	0.193	1.88	40.3	0.05	3.0E-06
		14.50	0.192	1.88	71.3	0.03	2.5E-06
	KCl	2.00	0.087	0.85	9.84	0.09	5.4E-06
	Saccharose	2.00	<0.01	<0.1	4.92	–	–
	PONPE10	4.00	<0.01	<0.1	9.84	–	1.3E-07
TM-2000	KCl	2.00	–	–	–	–	1.3E-05
		4.00	–	–	–	–	1.7E-05
		8.00	–	–	–	–	2.1E-05
	PONPE10	4.00	–	–	–	–	7.1E-06

osmotic pressure, which is compensated by the hydrostatic pressure varying with time:

$$h(t) = h_{max}\left[1 - e^{-t/\tau}\right]. \quad (5)$$

Here, h_{max} is the maximum liquid column height, t is the time, and τ is a parameter that depends on the membrane hydraulic permeability:

$$\tau = \frac{S_c}{L_p \rho g}. \quad (6)$$

Fitting the experimental $h(t)$ curves has shown that the growth of the solution column height with time is rather adequately described by Eq. (5). Approximation of the experimental data by an exponential function yields the numerical value of hydraulic permeability coefficient L_p, which characterizes the membrane upon the osmotic flow of water through its pores. To study the behavior of L_p in different regimes, the procedure of further experiments was modified as follows. At the first stage of the experiment, the varying solution column height $h(t)$ in the measuring capillary was monitored, when the left- and right-hand parts of the cell were filled with a studied solution and water, respectively. After the solution reached a level of h_{max}, water in the right-hand part of the cell was replaced by a solution equivalent to that located in the left-hand part, thereby equating the osmosity on both sides of the TM. At the second stage of the experiment, level $h'(t)$, which decreased under the action of the hydrostatic pressure, was measured. Typical results of such two-stage experiments are presented in Fig. 5 and Table 5. The decrease of the solution level in the descending branch of the curve obeys the following equation:

$$h'(t) = h_{max} e^{-\frac{t}{\tau 1}}, \quad (7)$$

where τ1 characterizes the hydraulic permeability of the membrane under the conditions of a viscous flow under the action of a hydrostatic pressure. The last column of Table 5 lists the values of pore radius r calculated from the L_p values by the Poiseuille equation

$$L_p = \frac{N\pi r^4}{8\mu l}. \quad (8)$$

Here, N is the number of pores in a sample and μ is the dynamic viscosity coefficient. The viscosities of the solutions were taken equal to the viscosity of water at the experiment temperature. The difference between the viscosities was negligible because of the low con-

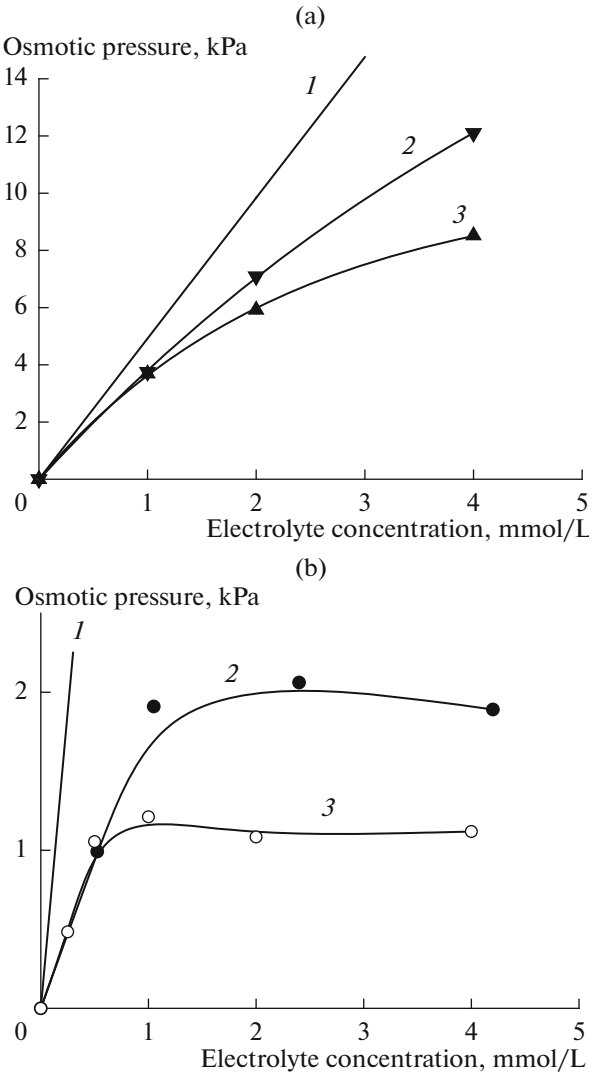

Fig. 4. Panel (a): dependences of measured osmotic pressure on concentration of 1 : 1 electrolytes (*2*) SDS and (*3*) KCl, straight line *1* corresponds to the ideal osmotic pressure of a 1 : 1 electrolyte. The TM-25 membrane is under examination. Panel (b): the same as in panel (a) for 1 : 2 electrolytes (*2*) SDDD and (*3*) K_2SO_4. The TM-100 membrane is under examination.

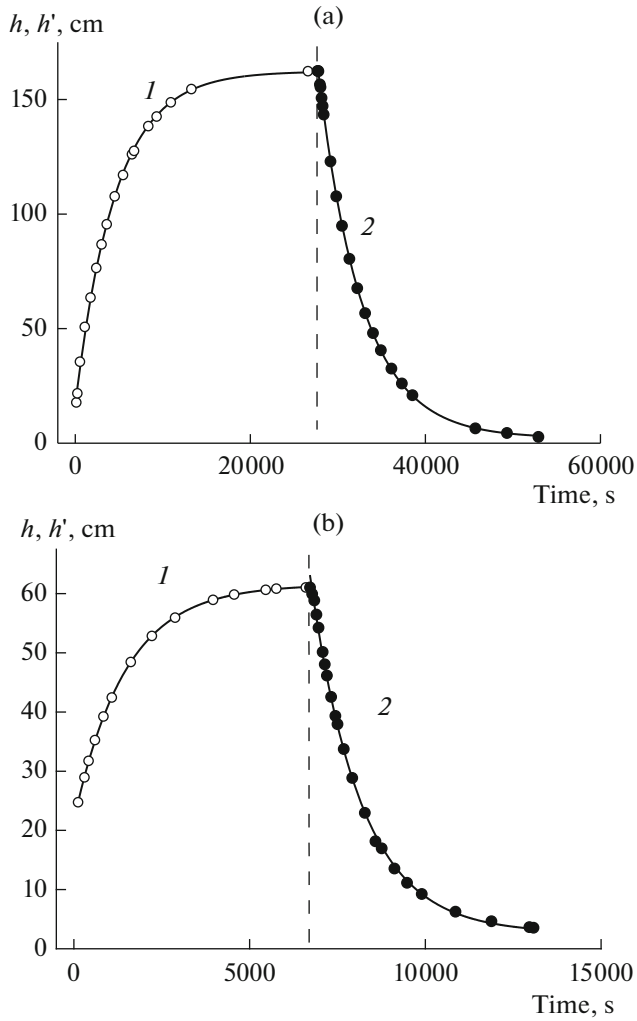

Fig. 5. Results of measuring TM permeability upon the osmotic flow (ascending branch of the $h(t)$ function, curve *1*) and under the action of hydrostatic pressure (descending branch of the $h'(t)$ function, curve *2*). Points and solid lines refer to experimental data and approximations by Eqs. (5) and (7), respectively: (a) 4 mmol/L K_2SO_4 solution and the TM-25 membrane and (b) 4 mmol/L KCl solution and the TM-40 membrane.

centrations of the solutions, including surfactant solutions [37].

As can be seen in Table 5, the hydraulic permeability of the membranes is almost the same at both stages of the experiment and corresponds to the viscous flow regime. Thus, the osmotic flow through TM pore channels is convective rather than diffusion. On the contrary, the authors of [15], using a set of Nuclepore TMs and a solution of a high-molecular-mass compound, which did not penetrate into the pores, revealed that the hydraulic permeability upon the osmotic flow is directly proportional to the effective area of the pores, i.e., to factor $N\pi r^2$. It was inferred from this finding that water transport through the pores corresponded to the diffusion mechanism. Our results evidently indicate the opposite situation; i.e., the osmotic pressure generated at a membrane/salt solution interface causes a viscous flow, for which the hydraulic permeability is proportional to $N\pi r^4$. Note that, in our experiments, no electroviscous effect was revealed; the Poiseuille pore radius determined for water and salt solution flows under both symmetric and asymmetric conditions was the same within the measurement error. If the apparent change in the viscosity was as small as a few percent, it could not be reliably detected in these experiments.

The effective pore radii calculated for the TM-25 and TM-40 membranes from the hydraulic permeability are, on average, approximately 1.8 nm smaller,

Table 5. Hydraulic permeability of TMs and effective pore radii upon flows induced by osmotic and hydrostatic pressures

Membrane	Phase compositions on different sides of a membrane	τ, s	τ1, s	L_p, 10^{-14} m^4 s kg^{-1}	r, nm
TM-25	4 mM KCl/H_2O	4298 ± 54		1.87	12.0
	4 mM KCl/4 mM KCl		4387 ± 32	1.83	11.9
	4 mM SDS/H_2O	8116 ± 48		0.99	10.1
	4 mM SDS/4 mM SDS		9141 ± 96	0.88	9.8
	4 mM K_2SO_4/H_2O	4605 ± 84		1.74	11.8
	4 mM K_2SO_4/4 mM K_2SO_4		4989 ± 27	1.61	11.6
TM-40	4 mM K_2SO_4/H_2O	1245 ± 24		6.45	21.5
	4 mM K_2SO_4/4 mM K_2SO_4		1265 ± 12	6.35	21.4
	4 mM SDS/H_2O	2012 ± 86		3.99	19.2
	4 mM SDS/4 mM SDS		1853 ± 46	4.33	19.6
	4 mM KCl/H_2O	1451 ± 8		5.53	21.0
	4 mM KCl/4 mM KCl		1438 ± 27	5.58	21.0
TM-100	4 mM SDS/H_2O	100.0 ± 2.0		80.2	49.4
	4 mM SDS/4 mM SDS		91.9 ± 5.6	87.3	50.5

Errors resulting from dispersions of experimental points for τ and τ1 values are shown in the table. Other sources of the errors (pore density, sample area, and membrane thickness) are the same for each pair of τ and τ1 values and, therefore, are ignored.

when SDS is used as an electrolyte (see the last column in Table 5). This may indicate that the layer of SDS adsorbed on the walls narrows the flow section of a pore.

It is of interest to compare the absolute values of water flow and salt counter flux under the conditions of osmosis. For example, in the case of the TM-25 membrane and a 2 mmol/L K_2SO_4 solution, the osmotic flow of water has, during initial several minutes of an experiment, a value of 5×10^{-6} mol/s, while the counter diffusion flux of the salt is only 2.5×10^{-10} mol/s. Thus, the ratio between the solvent flow and solute flux is higher than 10^4 and, on the order of magnitude, approximately corresponds to the ratio between their molar fractions in the solution. Taking the pore radius equal to ~10 nm, it is easy to calculate water flow velocity v averaged over the pore cross section. In this experiment, it was nearly 1×10^{-3} cm/s. Longitudinal salt concentration profile $c(x)$ in a cylindrical pore under the conditions of simultaneous diffusion flux and convective flow may be approximately estimated by solving the following equation [17]:

$$-\frac{v}{D}\frac{dc}{dx} = \frac{d^2c}{dx^2}, \quad (9)$$

where D is the diffusion coefficient of a solute in a pore. This equation has been written under simplifying assumptions that the diffusion coefficient is independent of concentration, while the concentration is averaged over the cross section of the pore; that is, it depends on x alone. As has been shown in [17], if parameter v/D is lower than 1000 cm^{-1}, the concentration gradient in a pore is almost linear, and the convective flow has no effect on the diffusion rate. If we take volume values for the diffusion coefficient of the used salts, condition $v/D < 1000$ is always fulfilled at convection velocity $v = 1 \times 10^{-3}$ cm/s. Indeed, in the majority of our experiments, the salt concentration in the right-hand part of the cell grew at an almost constant rate irrespective of the velocity of the osmotic counter flow (see Fig. 3b). However, in some cases (4 mmol/L SDS, TM-25 and 8 mmol/L SDS, TM-40) we observed a reliable enhancement of the diffusion flux by 10–20%, and this enhancement correlated with a decrease in the osmotic flow. Seemingly, the initial velocity of the convective flow was, under these conditions, sufficiently high to affect diffusion. At the same time, the diffusion coefficients in nanopores are substantially lower than the volume values, which is evident from the data presented in the last columns of Tables 2–4 and published data [23].

Note that the ionic selectivity and reverse-osmotic properties of fine-pore TMs were revealed and studied rather long ago. For this purpose, membranes with effective pore diameters of 8 and 3 nm prepared by special methods—thermal shrinkage of a typical TM or extraction of a low-molecular-mass fraction from a PET film irradiated by heavy ions—were used [10, 38]. In later work [39], the selectivity with respect to KCl solutions (2.5 and 10 mmol/L) was studied for a TM that had parameters very close to those of our TM-25 sample. However, the process of the direct osmosis in

the TM has, so far, been ignored. In the literature, we have found only one cursory mention of the necessity to take into account this effect [35] when measuring the membrane potential.

In connection with the interpretation of our data, it is necessary to mention the phenomenon of capillary osmosis. The capillary osmosis theory has been developed for wider capillaries, in which the liquid transport has the character of a capillary-osmotic slip [40]. Experiments on the capillary osmosis in electrolyte solutions were performed for pores with radii nearly two orders of magnitude larger than those in our TM samples [41]. At $\Delta c = 10^{-3}$–0.5 mmol/L, the velocity of the capillary-osmotic transport had an order of 10^{-5} cm/s and weakly depended on concentration. The character of the osmotic flow through nanopores in our TM samples (Poiseuille flow with a velocity of $\sim 10^{-3}$ cm/s and above) shows that, when the thickness of diffuse ionic layers is comparable with or larger than the capillary radius, a different model is required.

Several theoretical models have been reported, which describe osmosis in nanopores or nanochannels with charged walls (see, e.g., [42–45]). In this work, we do not intend to analyze in detail the results from the point of view of their correspondence to this or that model. At this stage of the study, it seems to be of importance to focus attention on the fact that TMs with pore radii of 10–50 nm are convenient objects for studying osmotic effects caused by electrolyte concentration gradients. The regular cylindrical geometry of the pores has given opportunity to identify the Poiseuille flow regime, which is an indicator of a parabolic distribution of liquid flow velocities in a pore, while the theory predicts, generally speaking, a different shape of the velocity profile [5, 42, 45]. The use of the ionic surfactant has made it possible to observe effects associated with changes in surface charge density. The application of this possibility in subsequent experiments with TMs, the widening of the range of the studied concentrations, and the use of other electrolytes, in particular, 2 : 1 electrolytes, will yield additional criteria, which may be employed to judge the adequacy of this or that model.

Moreover, a deeper insight into the physicochemical processes in nanocapillaries in the presence of solute concentration gradients is of importance in connection with specific practical problems. For example, the targeted application of osmotic effects enables one to control the shape of asymmetric nanopores [17] used as working elements of molecular sensors.

The confirmation obtained in this work that a decisive role is played by EDLs may contribute to understanding osmotic phenomena accompanying asymmetric etching of heavy-ion tracks. Conical pores resulting from this process have a low resistance to viscous flow. Therefore, the velocity of a convective flow in a pore mouth may be sufficiently high to provide the dilution of an electrolyte and the thickening of an EDL to a size comparable with the mouth radius in spite of the fact that concentrated solutions are used for etching.

4. CONCLUSIONS

Most studies of osmotic phenomena have been carried out with semipermeable membranes. In this work, we investigated osmotic flows through track-etched (i.e., capillary-porous) membranes and have shown that, at electrolyte concentrations ensuring EDL thicknesses comparable with pore radii, the osmotic transport of water may be substantial. The necessary membrane selectivity is completely provided by its surface electric charge. The charge density may be additionally increased by using a solution of an ionic surfactant. The proper geometry of pores in TMs has made it possible to perform experiments aimed to clarify the mechanism of the flow caused by an osmotic driving force. These experiments have shown that the osmotic flow through nanocapillaries with radii of 10–50 nm is purely convective.

ACKNOWLEDGMENTS

We are grateful to O.L. Orelovitch and N.E. Lizunov for help in studying TMs by SEM.

REFERENCES

1. Wijmans, J.G. and Baker, R.W., *J. Membr. Sci.*, 1995, vol. 107, p. 1.
2. Cath, T.Y., Childress, A.E., and Elimelech, M., *J. Membr. Sci.*, 2006, vol. 281, p. 70.
3. Mauro, A., Science (Washington, D. C.), 1957, vol. 126, p. 252.
4. Anderson, J.L. and Malone, D.M., *Biophys. J.*, 1974, vol. 14, p. 957.
5. Marshall, E.A., *J. Theor. Biol.*, 1977, vol. 66, p. 107.
6. Thomas, S.R. and Mikulecky, D.C., *Microvasc. Res.*, 1978, vol. 15, p. 207.
7. Schultz, J.S., Valentine, R., and Choi, C.Y., *J. Gen. Physiol.*, 1979, vol. 75, p. 49.
8. Hill, A., *Proc. R. Soc. London*, 1989, vol. 237, p. 369.
9. Hill, A., *J. Membr. Biol.*, 1994, vol. 137, p. 197.
10. Yaroshchuk, A.E., *Adv. Colloid Interface Sci.*, 1995, vol. 60, p. 1.
11. Guell, D.C. and Brenner, H., *Ind. Eng. Chem. Res.*, 1996, vol. 35, p. 3004.
12. Kramer, E.M. and Myers, D.R., *Am. J. Phys.*, 2012, vol. 80, p. 694.
13. Kramer, E.M. and Myers, D.R., *Trends Plant Sci.*, 2013, vol. 18, p. 195.
14. Zeman, L. and Wales, M., *Sep. Sci. Technol.*, 1981, vol. 16, p. 275.
15. Comper, W.D. and Williams, R.P.W., *Biophys. Chem.*, 1990, vol. 36, p. 215.

16. Apel, P.Y., Bashevoy, V.V., Blonskaya, I.V., Lizunov, N.E., Olejniczak, K., Orelovitch, O.L., and Trautmann, C., *Phys. Chem. Chem. Phys.*, 2016, vol. 18, p. 25421.
17. Apel, P.Y., Blonskaya, I.V., Lizunov, N.E., Olejniczak, K., Orelovitch, O.L., Tomil-Molares, M.E., and Trautmann, C., *Small*, 2018, vol. 14, p. 1703327.
18. Apel, P.Yu., Korchev, Yu.E., Siwy, Z., Spohr, R., and Yoshida, M., *Nucl. Instrum. Methods Phys. Res. B*, 2001, vol. 184, p. 337.
19. Gusinskii, G.M., Kremer, E.B., Kremer, M.I., and Mchedlishvili, B.V., *Inzh.-Fiz. Zh.*, 1979, vol. 37, p. 1119.
20. Apel, P., *Radiat. Meas.*, 2001, vol. 34, p. 559.
21. Beck, R.E. and Schultz, J.S., *Biochim. Biophys. Acta*, 1972, vol. 255, p. 273.
22. *Encyclopedia of Membrane Science and Technology*, Hoek, E.M.V. and Tarabara, V.V., Eds., New Jersey: Wiley, 2013, p. 332.
23. Schoenenberger, C., Van der Zande, B.M.I., Fokkink, L.G.J., Henny, M., Schmid, C., Krueger, M., Bachtold, A., Huber, R., Birk, H., and Staufer, U., *J. Phys. Chem. B*, 1997, vol. 101, p. 5497.
24. Yamauchi, Yu., Blonskaya, I.V., and Apel', P.Yu., *Colloid J.*, 2017, vol. 79, p. 707.
25. Plecis, A., Schoch, R.B., and Renaud, P., *Nano Lett.*, 2005, vol. 5, p. 1147.
26. Lück, H.B., *Nucl. Instrum. Methods Phys. Res.*, 1983, vol. 213, p. 507.
27. Apel, P.Yu. and Pretzsch, G., *Nucl. Tracks Radiat. Meas.*, 1986, vol. 11, p. 45.
28. Berezkin, V.V., Kiseleva, O.A., Nechaev, A.N., Sobolev, V.D., and Churaev, N.V., *Kolloidn. Zh.*, 1994, vol. 56, p. 319.
29. Geissman, C. and Ulbricht, M., *Macromol. Chem. Phys.*, 2005, vol. 206, p. 268.
30. Dejardin, P., Vasina, E.N., Berezkin, V.V., Sobolev, V.D., and Volkov, V.I., *Langmuir*, 2005, vol. 21, p. 4680.
31. Yaroshchuk, A.E., Zhukova, O., Ulbricht, M., and Ribitsch, V., *Langmuir*, 2005, vol. 21, p. 6872.
32. Cervera, J., Alcaraz, A., Schiedt, B., Neumann, R., and Ramirez, P., *J. Phys. Chem. C*, 2007, vol. 111, p. 12265.
33. Xue, J., Xie, Y., Yan, Y., Ke, J., and Wang, Y., *Biomicrofluidics*, 2009, vol. 3, p. 022408.
34. Keesom, W.H., Zelenka, R.L., and Radtke, C.J., *J. Colloid Interface Sci.*, 1988, vol. 123, p. 575.
35. Sidorova, M.P., Ermakova, L.E., Savina, I.A., and Mchedlishvili, B.V., *Kolloidn. Zh.*, 1990, vol. 52, p. 895.
36. Yamauchi, Yu. and Apel, P.Yu., *Colloid J.*, 2017, vol. 79, p. 286.
37. Ito, T. and Mizutani, Y., *Jpn. Oil Chem. Soc.*, 1968, vol. 17, p. 246 (in Japanese).
38. Berezkin, V.V., Nechaev, A.N., Fomichev, S.V., Mchedlishvili, B.V., and Zhitaryuk, N.I., *Kolloidn. Zh.*, 1991, vol. 53, p. 339.
39. Yaroshchuk, A., Boiko, Y., and Makovetsky, A., *Langmuir*, 2009, vol. 25, p. 9605.
40. Derjaguin, B.V., Churaev, N.V., and Muller, V.M., *Surface Forces*, New York: Consultants Bureau, 1987.
41. Derjaguin, B.V., Koptelova, M.M., Muller, V.M., and Tikhomolova, K.P., *Kolloidn. Zh.*, 1977, vol. 39, p. 1060.
42. Sasidhar, V. and Ruckenstein, E., *J. Colloid Interface Sci.*, 1981, vol. 82, p. 439.
43. Sasidhar, V. and Ruckenstein, E., *J. Colloid Interface Sci.*, 1982, vol. 85, p. 332.
44. Qian, S., Das, B., and Luo, X., *J. Colloid Interface Sci.*, 2007, vol. 315, p. 721.
45. Liu, K.-L., Hsu, J.-P., and Tseng, S., *Langmuir*, 2013, vol. 29, p. 9598.

Translated by A. Kirilin